Supplement of Atmos. Chem. Phys., 26, 2319–2329, 2026
https://doi.org/10.5194/acp-26-2319-2026-supplement

Atmospheric Chemistry and Physics
Open Access
EGU

Supplement of

Temperature–RH dependent viscosity of organic aerosols from 273 to 303 K: implications for global N_2O_5 uptake

Atta Ullah et al.

Correspondence to: Mijung Song (mijung.song@jbnu.ac.kr)

S1. Flow-cell calibration and particle conditioning time determination

In both bead-mobility and poke-and-flow experiments, the flow-cell was calibrated for relative humidity (RH) using the deliquescence points of three salts, including K_2CO_3, NaCl, and $(NH_4)_2SO_4$ (Winston and Bates, 1960). The experimentally determined deliquescence RH values at each measurement temperature of 273, 283, 293, and 303 K were compared with the literature. The RH measurement uncertainty was quantified as the temperature-dependent calibration root mean square error of the RH sensor. The RH accuracy was within ± 2.0% at 293 K, and the temperature was controlled within ± 1 K of the target.

Prior to each experiment, particles deposited on a hydrophobic substrate were conditioned at the target RH of the carrier gas to allow sufficient equilibration with the surrounding gases. Conditioning times were adjusted depending on the experimental temperature and technique. To evaluate whether the samples reached near-equilibrium with the target RH, we applied a method previously reported in the literature (Evoy et al., 2021; Maclean et al., 2021; Smith et al., 2021; Kiland et al., 2023). This method involves comparing experimental conditioning time to the characteristic mixing time of water within organic aerosol (OA), τ_{mix,H_2O}, calculated:

$$\tau_{mix,H2O} = \frac{{d_p}^2}{4\pi^2 D_{H2O}(T,RH)} \quad \text{(S1.1)}$$

Here, d_p represents the particle diameter. $D_{H_2O}(T,RH)$ is the RH- and temperature-dependent diffusion coefficient of water in OA. The value of D_{H_2O} was calculated using the fractional Stokes–Einstein equation, which accounts for the link between viscosity and diffusion in cases where the diffusing species are comparable in size to, or smaller the surrounding matrix molecules (Evoy, 2020):

$$D_{H2O}(T,RH) = D°_{H2O}(T) \times \left(\frac{\eta°_{H2O}(T)}{\eta(T,RH)}\right)^{\xi} \quad \text{(S1.2)}$$

In this equation, $D°_{H2O}(T)$ is the self-diffusion of water calculated with the Stokes-Einstein equation at 293 K (2.15×10^{-9} m^2 s^{-1}). $\eta°_{H2O}(T)$ is the viscosity of pure water obtained from literature with values of 1.78×10^{-3} Pa·s at 273 K, 1.31×10^{-3} Pa·s at 283 K, 1×10^{-3} Pa·s at 293 K, and 8.14×10^{-4} Pa·s at 303 K (Weight, 2019). $\eta(T,RH)$ is the measured viscosity of sucrose-H_2O droplets at the corresponding RH and temperature. ξ is the fractional exponent, using Eq. (S1.3), which accounts for the relative size of the diffusing molecule and the matrix:

$$\xi = 1 - \left[A \times exp\left(-B\frac{r_{diff}}{r_{matrix}}\right)\right] \quad \text{(S1.3)}$$

where coefficient values of $A = 0.73$ and $B = 1.79$ (Evoy et al., 2020), r_{diff} hydrodynamic radius of water of 0.1 nm (Price et al., 2016). The matrix radius, r_{matrix}, of the sucrose molecule was calculated under the assumption of spherical geometry, using 342.30 g mol^{-1} and a density of 1.67 g cm^{-3} (Haynes, 2016), resulting in $r_{matrix} = 0.44$ nm and $\xi = 0.51$. Conditioning durations for the other temperatures (273, 283, 293, and 303 K) are summarized in Table S1.

In addition to water, we also estimated the mixing times of organic molecules ($\tau_{mix,org}$) to assess potential diffusion limitations within the particle matrix itself. This is particularly relevant under conditions where semi-solid or glassy states may impede equilibration. The diffusion coefficient of organics (D_{org}) was calculated using the classical Stokes–Einstein equation (Eq. S1.4) (Evoy et al., 2019; Evoy et al., 2020):

$$D_{org}(T, RH) = \frac{kT}{6\pi\eta_{org}(RH, T)R_{diff}} \quad \text{(S1.4)}$$

where k is the Boltzmann constant, η_{org} is the temperature- and RH-dependent viscosity of OA, and R_{diff} is the radius of the diffusing molecules. We used 0.4 nm for R_{diff}, consistent with typical organic molecules of similar molecular weight and density. Using the estimated diffusion coefficients, the mixing time of organics was calculated as:

$$\tau_{mix,org} = \frac{{d_p}^2}{4\pi^2 D_{org}(T, RH)} \quad \text{(S1.5)}$$

A particle diameter of 200 nm was used in all calculations, consistent with the typical size of secondary organic aerosol (SOA) particles observed in the atmosphere (Pöschl et al., 2010; Riipinen et al., 2011). The $\tau_{mix,org}$ value represents the time required for the concentration of the diffusing species at the particle's center to attain 1/e of the equilibrium concentration.

The diffusivity coefficient of N_2O_5 in OA, which is needed in calculations of N_2O_5 uptake coefficient, is also determined using the fractional Stokes-Einstein equation (S1.2 and S1.3). In Eq. (S1.3), the hydrodynamic radius of N_2O_5 is set to be 0.25 nm (Grzinic et al., 2015).

S2. Viscosity parameterization of sucrose-H_2O droplets

We parameterized the viscosity of sucrose-H_2O droplets as a function of RH and temperature, following the approach proposed by Kiland et al. (2023). Experimental data at 293 ± 1 K was fitted using a mole-fraction-based Arrhenius mixing rule (Eq. S2.1)

$$log\big(\eta(RH, 293K) = x_{org}\, log_{10}\big(\eta_{org,dry}\big) + \big(1 - x_{org}\big) log\big(\eta°_{H2O}\big) \tag{S2.1}$$

where $\eta(RH, 293K)$ is the viscosity of the mixture at room temperature, $\eta_{org,dry}$ is the viscosity of the organic component at 0% RH (1×10^{12} Pa·s), and $\eta°_{H_2O}$ is the viscosity of pure water (1×10^{-3} Pa·s).

The mole fraction of organic components, x_{org}, was calculated from the mass fraction using:

$$x_{org} = \frac{\frac{w_{org}}{M_{org}}}{\frac{w_{org}}{M_{org}} + \frac{1 - w_{org}}{M_{H_2O}}} \tag{S2.2}$$

where w_{org} is the mass fraction of the organic component, and M_{org} and M_{H_2O} are the molecular weights of sucrose and water, respectively. w_{org} was determined from the water activity (a_w = $RH/100$) using a mass-based hygroscopicity parameter κ, as shown in Eq. (S2.3).

$$w_{org} = \left(1 + \kappa \left(\frac{a_w}{1 - a_w}\right)\right)^{-1} \tag{S2.3}$$

Fitting the experimental data at 293 K yielded the value of κ = 0.061 ± 0.0023. As shown in Fig. S8, the model provides a good fit to the experimental data, supporting the robustness of the parameterization. Petters and Kreidenweis (2007) reported κ values between 0.01 and 0.5 for diverse organic compounds, highlighting variability in hygroscopicity with molecular structure.

S3. Determination of D_f using global fitting of viscosity data

To determine a single value of D_f, we performed a global fit of all viscosity measurements to Eq. (1), First, we compiled all viscosity data points measured at different combinations of RH and Temperature. Second, for each data point, we calculated $T_o(RH)$ using the RH-dependent parameterization described in Sect. S2. Third, we fitted (Eq. 1) simultaneously to the entire dataset using a nonlinear least-squares routine, minimizing the sum of squared differences between measured and modelled $ln\ \eta(RH,\ T)$. In this global fit, D_f was treated as the single free parameter (while $\eta\infty$ was fixed), so that one best-fit value of D_f characterizes the overall temperature sensitivity of viscosity across all RH conditions.

The fragility parameter we derived is indicative of the unique molecular interactions and hydration properties found in sucrose-rich particles. These particles are characterized by sharp changes in viscosity with temperature near their glass transition point. This accounts for our slightly higher fragility value compared to the lower limit reported by Derieux et al. (2018), who studied a wider variety of organic aerosol surrogates with more complex functional groups, resulting in a broader range of thermodynamic behaviors. The difference in fragility values does not represent a contradiction but rather highlights the influence of composition. Systems dominated by sucrose typically show greater sensitivity to temperature variations near Tg than mixtures containing many functional groups, leading to higher measured fragility.

To assess sensitivity to uncertainty in the fragility parameter, calculations using $D_f = 13$ and 10 were compared (Fig. S12). The predicted latitude–altitude patterns of viscosity and $\tau_{mix,org}$ of sucrose-H_2O droplets were broadly similar, indicating that the large-scale phase-state structure was relatively robust to the assumed D_f. Nevertheless, these results should be interpreted in light of the study's limitations, as the viscosity parameterization is extrapolated beyond 273–303 K, where sensitivities to RH and meteorological averaging increase.

S4. Collection of global ambient zonal RH and temperature

To evaluate the tropospheric distribution of predicted sucrose-H_2O droplet phase state and mixing times, we utilized monthly mean reanalysis data for temperature and RH from the Copernicus Climate Data Store (https://cds.climate.copernicus.eu/) (Hersbach et al., 2023). Monthly mean temperature and RH on pressure levels were obtained from the ERA5 reanalysis (Copernicus Climate Data Store) for 2020–2024. Latitude–altitude profiles were constructed by averaging across all longitudes at each latitude and pressure level. Pressure levels were converted to geometric altitude using the barometric (hypsometric) relationship (Eq. S4.1), and the resulting zonal-mean profiles are shown in Fig. S9. The dataset provides global coverage from 90°N to 90°S and 180°W to 180°E, with temporal resolution spanning January 2020 to December 2024. To convert pressure-level data to geometric altitude, Eq. (S4.1) represents the hypsometric relationship assuming a constant temperature lapse rate. This formulation is widely used to visualize the pressure-level meteorological data on an altitude coordinate and does not alter the underlying temperature or RH values (Maclean et al., 2021; Kiland et al., 2023). In this framework, the height (h) associated with each pressure level was then calculated using the given Eq. (S4.1), the hypsometric form of the barometric equation, which relates the vertical spacing between the pressure surfaces to the mean temperature of the air column between them.

$$h = \frac{1 - \left(\frac{P}{P_o}\right)^{\frac{R\lambda}{M_{air}}}}{\lambda / T_o} \tag{S4.1}$$

where P is the pressure at the given level (1000 hPa – 100 hPa), p_o is the pressure at sea level (101325 Pa), R is the gas constant (8.314 J mol^{-1} K^{-1}), λ is the temperature lapse rate (6.5 K km^{-1}), M_{air} is the molecular mass of the air (28.97 g mol^{-1}), and T_o is the mean temperature at the surface (288.15 K). To construct latitude–altitude profiles, the monthly RH and temperature values were averaged across all longitudes at each latitude and pressure level.

S5. Detailed formulation of the N_2O_5 uptake calculation

To calculate the N_2O_5 uptake coefficient on sucrose-H_2O droplets ($\gamma_{N_2O_5}$), we used a resistor-model framework following Ammann et al. (2013) and Gržinić et al. (2015), identical to the formulation employed in our previous work (Song et al., 2025). The overall uptake coefficient is given by Eq. (S5.1).

$$\frac{1}{\gamma_{N_2O_5}} = \frac{1}{\alpha_s} + \frac{1}{\Gamma_s + \left(\frac{1}{\Gamma_{sb}} + \frac{1}{\Gamma_b}\right)^{-1}} \quad \text{(S5.1)}$$

where α_s is the accommodation coefficient, Γ_s represents the limiting uptake coefficient for the surface reaction, Γ_{sb} accounts for surface to bulk transport, and Γ_b describes limitations associated with bulk diffusion and chemical reaction within the particle. For organic aerosols exhibiting high viscosity, previous studies have shown that Γ_b typically dominates the overall resistance, whereas surface-related terms contribute comparatively weakly to the humidity dependence of $\gamma_{N_2O_5}$.

The bulk resistance term, Γ_b, is calculated using a reacto-diffusive formulation (Eq. S5.2):

$$\frac{1}{\Gamma_b} = \frac{\omega}{4HRT\sqrt{D_{N2O5}k^I}}(\coth q - \frac{1}{q})^{-1} \quad \text{(S5.2)}$$

where ω is the mean thermal velocity of N_2O_5, H is the Henry's law constant, R is the ideal gas constant, T is the temperature, $D_{N_2O_5}$ is the diffusion coefficient of N_2O_5 in the particle phase, and k^I is the first-order hydrolysis rate constant. The reacto-diffusive parameter (q) is defined as r/l, where r is the particle radius, and l is the reacto-diffusive length given by $\sqrt{D_{N_2O_5}/k^I}$. This formulation explicitly links aerosol viscosity to N_2O_5 uptake through its control on $D_{N_2O_5}$ and thus on the penetration depth of N_2O_5 into the particle prior to reaction.

The surface accommodation coefficient (α_s) was set to 1, such that surface accommodation does not limit uptake and Γ_s was set to 2.5×10^{-4} based on previous simulations and observations at low RH conditions (Grzinic et al., 2015). This value shows a typical, experimentally supported lower bound for surface-limited uptake and contributes substantially only when bulk diffusion is suppressed, that is, under conditions of high viscosity. At moderate to high RH, where viscosity is low and diffusion is rapid, the surface term becomes negligible relative to bulk resistance. The bulk accommodation coefficient was set to $\alpha_b = 0.035$ following the recommendation of Ammann et al. (2013), representing the effective probability of N_2O_5 entering the particle phase prior to hydrolysis.

The diffusion coefficient of N_2O_5 in the particle phase was determined from viscosity using a fractional Stokes–Einstein relationship. A fractional exponent of 0.74 was adopted, calculated from literature-derived parameters using the equations described in Sect. S1. In this calculation, the molecular radius of N_2O_5 was taken as 0.25 nm

(Grzinic et al., 2015), and the matrix radius was set to 0.44 nm, corresponding to the effective molecular size of sucrose.

The intrinsic first-order hydrolysis rate constant (k^I) was set to 4.1 ns, based on recent molecular dynamics simulations of N_2O_5 hydrolysis in bulk water (Galib and Limmer, 2021). Although this value was derived under aqueous conditions at room temperature, it provides a physically reasonable estimate of intrinsic chemical reactivity once N_2O_5 is solvated. Using the viscosity-derived diffusion coefficients, the reacto-diffusive length and the corresponding reacto-diffusive parameter were calculated and subsequently applied in Eqs. (S5.1) and (S5.2) to determine $\gamma_{N_2O_5}$ across the tropospheric temperature and RH.

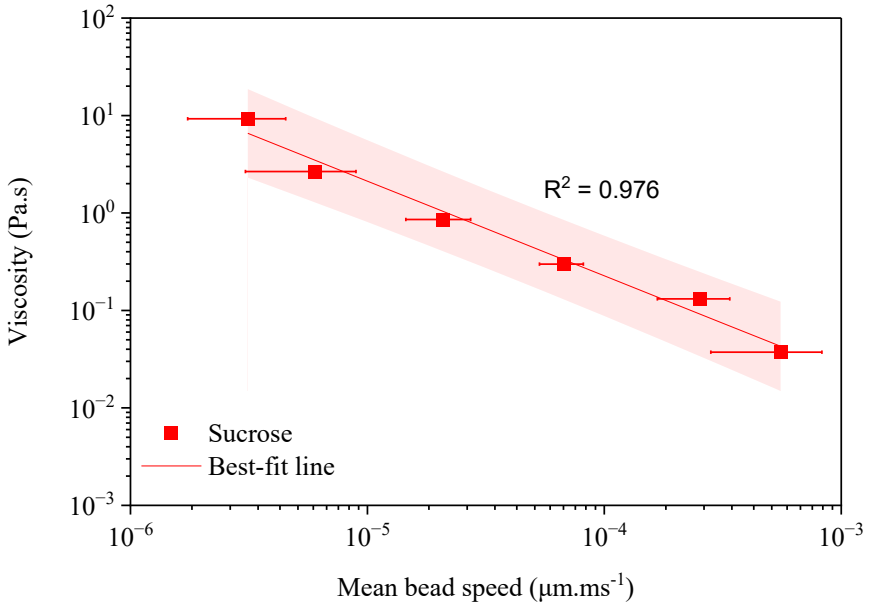

Figure S1. Calibration line illustrating the relationship between mean bead speeds and viscosities of sucrose-H_2O droplets at varying relative humidity (RH) levels. A linear regression, shown by the red solid line, fits the data with the equation: $viscosity = 0.00003 \times (mean\ bead\ speed)^{-0.971}$. The pink area denotes 95% prediction bands of fitting to the data in this study. The uncertainty in mean bead speed along the *x–axis* is calculated from standardization of 2–5 beads within 3–5 particles for each RH value.

Temp	Particle position 1	Particle position 2	Particle position 3
273 K, ~80% RH	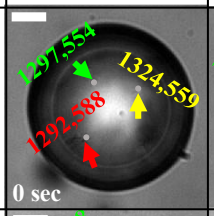	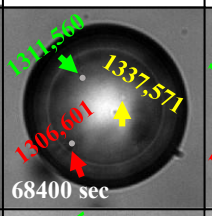	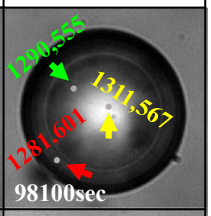
283 K, ~80% RH	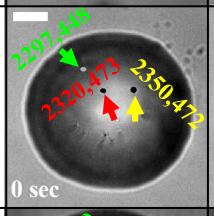	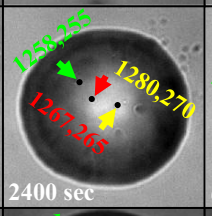	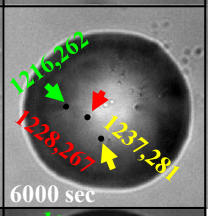
293 K, ~80% RH	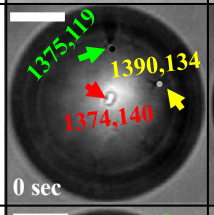		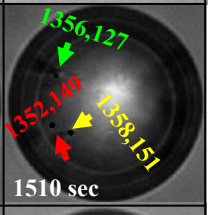
303 K, ~73% RH	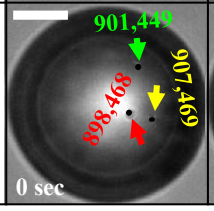	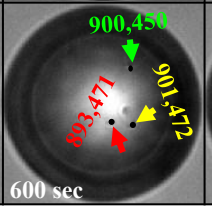	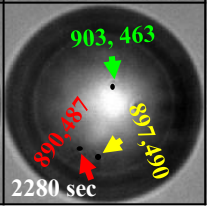

Figure S2. Optical images of sucrose-H_2O droplets during a typical bead-mobility experiment at different temperatures. Three labeled beads with tracked *x* and *y* coordinates were used to determine average bead speeds using ImageJ software. The size of the scale bar is 20 µm.

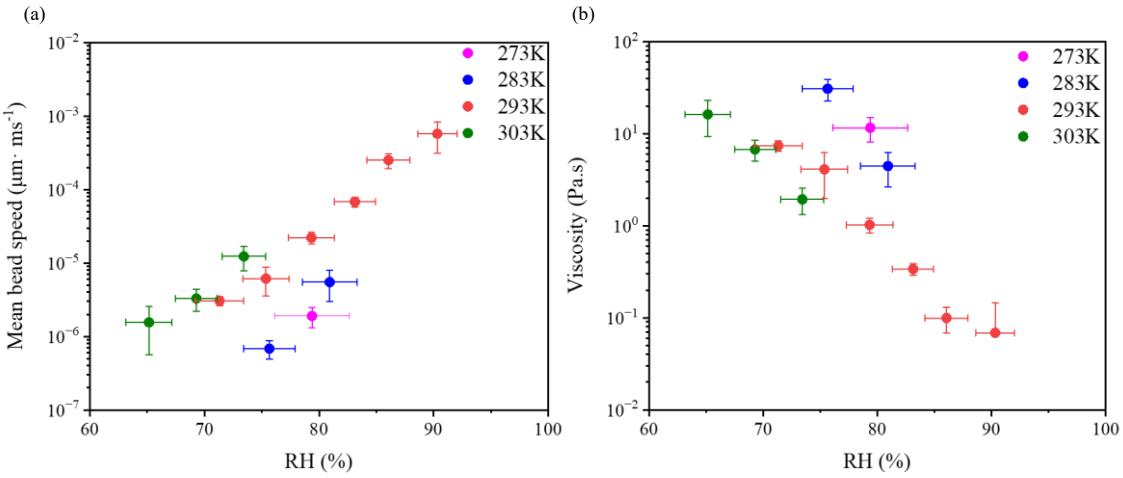

Figure S3. (a) Mean bead speed and (b) resulting viscosities from bead-mobility experiments for sucrose-H_2O droplets as a function of temperature and relative humidity (RH). The *x*-axis error bars represent the RH range in a given experiment and the uncertainty in RH measurements. The *y*-axis error bars indicate the standard deviation of the measured bead speeds and viscosity calculated from 3–5 beads across 2–5 particles at each RH level.

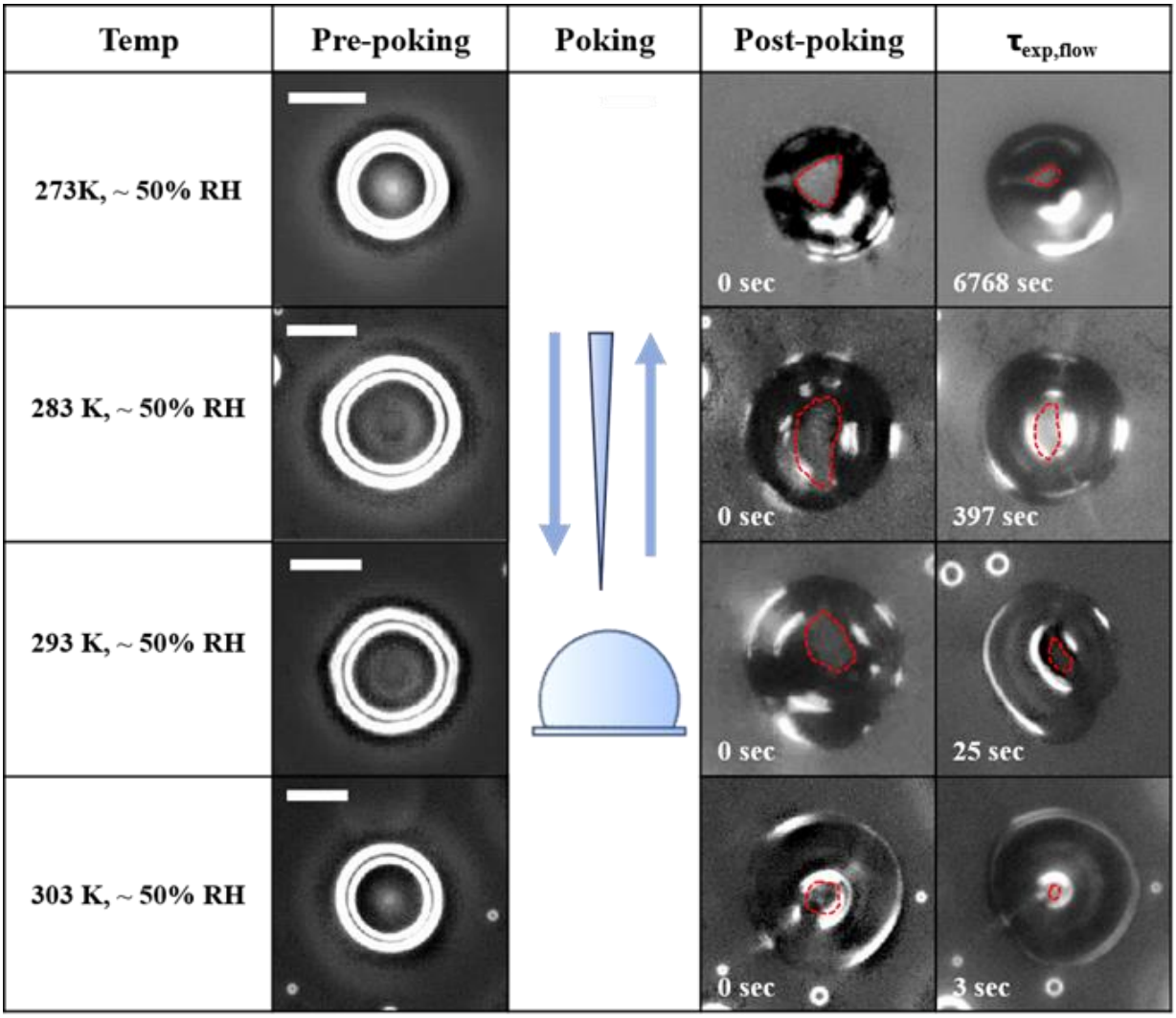

Figure S4. Optical images for experimental flow times ($\tau_{exp,flow}$) during poke-and-flow experiments at different temperatures. The white scale bar indicates 20 μm. The red dotted lines indicate the size of the cavity measured at the corresponding time after poking.

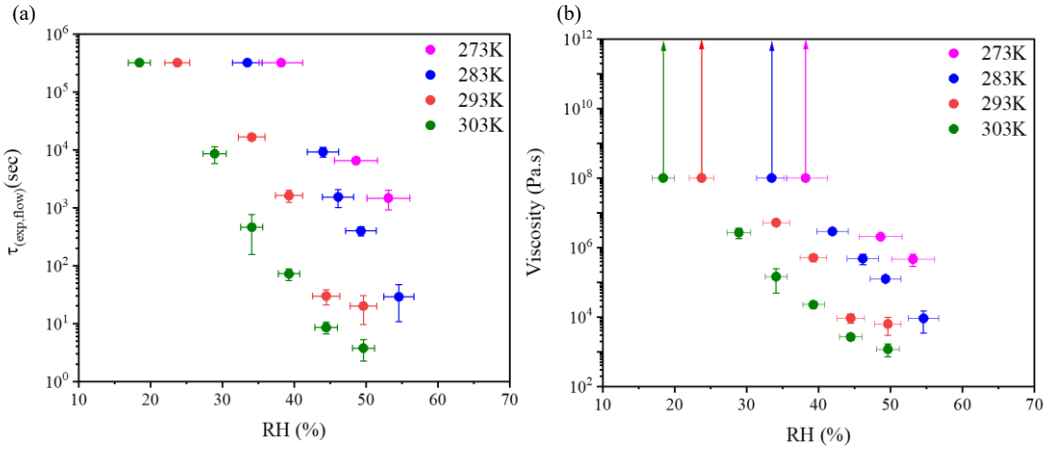

Figure S5. (a) Mean experimental flow time ($\tau_{exp,\ flow}$) from poke-and-flow experiments for sucrose-H_2O droplets as a function of temperature and relative humidity (RH). The *x*-axis error bars represent the RH range in a given experiment and the uncertainty in RH measurements. The *y*-error bars indicate the standard deviation of the measured $\tau_{exp,\ flow}$ calculated from measurements of 3–4 particles at each RH level. (b) Resulted viscosities from the $\tau_{exp,\ flow}$ using the equation proposed by Sellier et al. (2015). The *y*-error bars indicate the standard deviation of the measured viscosity.

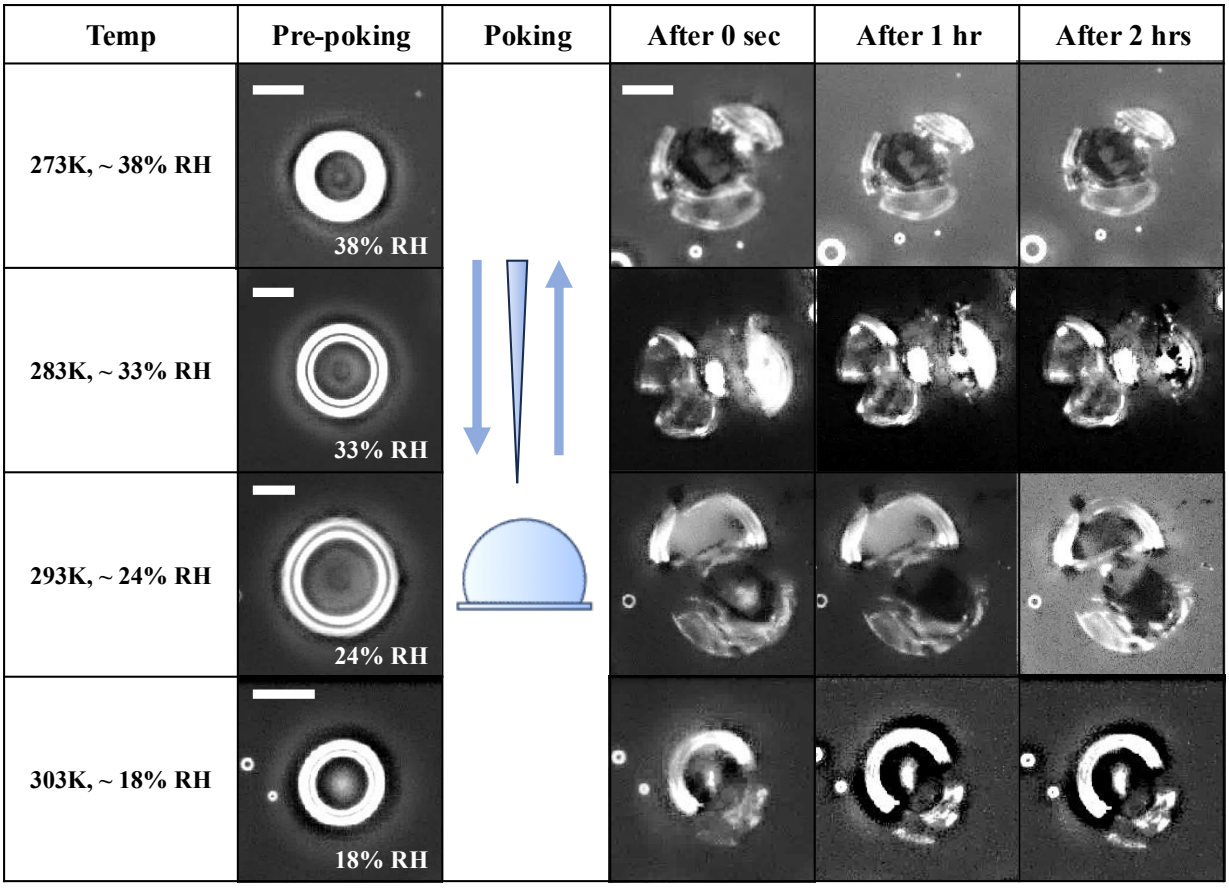

Figure S6. Optical images of sucrose-H_2O droplets during poke–and–flow experiments at different temperatures. Observations were made when particles cracked at a certain relative humidity (RH), and they were then monitored for longer than 2 hours, with no evidence of flow restoration was detected. RH was consistently regulated throughout the pre-poking, poking, and post-poking stages. White scale bars represent 20 µm.

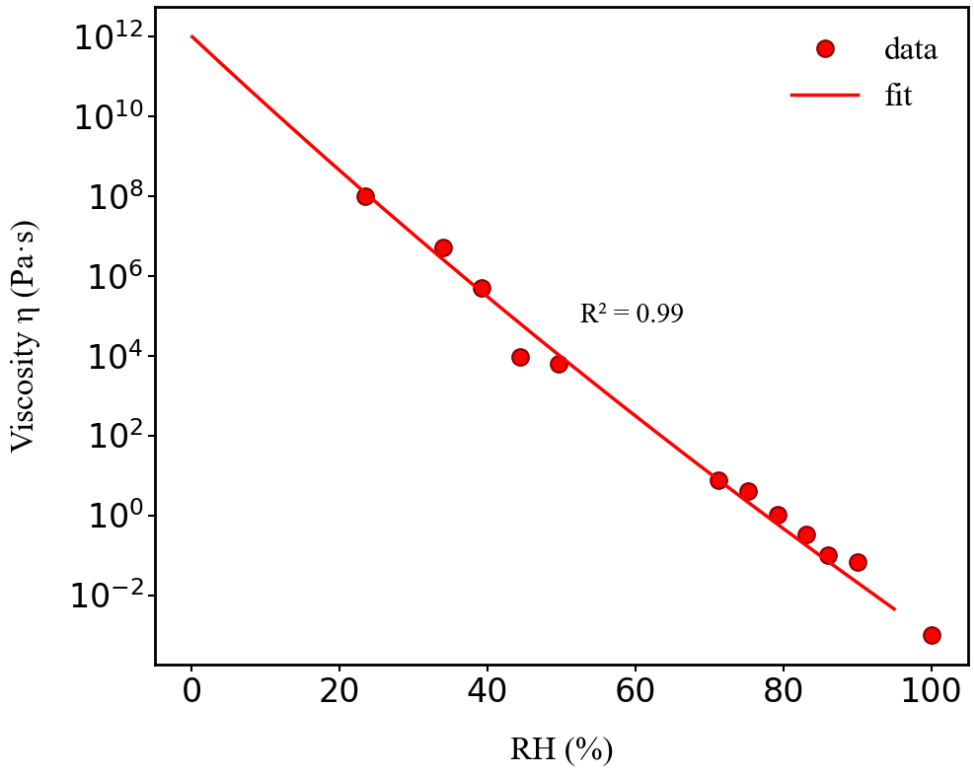

Figure S7. The viscosity of sucrose-H_2O droplets as a function of RH at room temperature. The solid line is a mole-fraction-based Arrhenius mixing rule fit to the viscosity data (Eq S2.1), which yields a hygroscopicity parameter, κ = 0.061 ± 0.0023. The point at 100% RH represents the viscosity of water at room temperature.

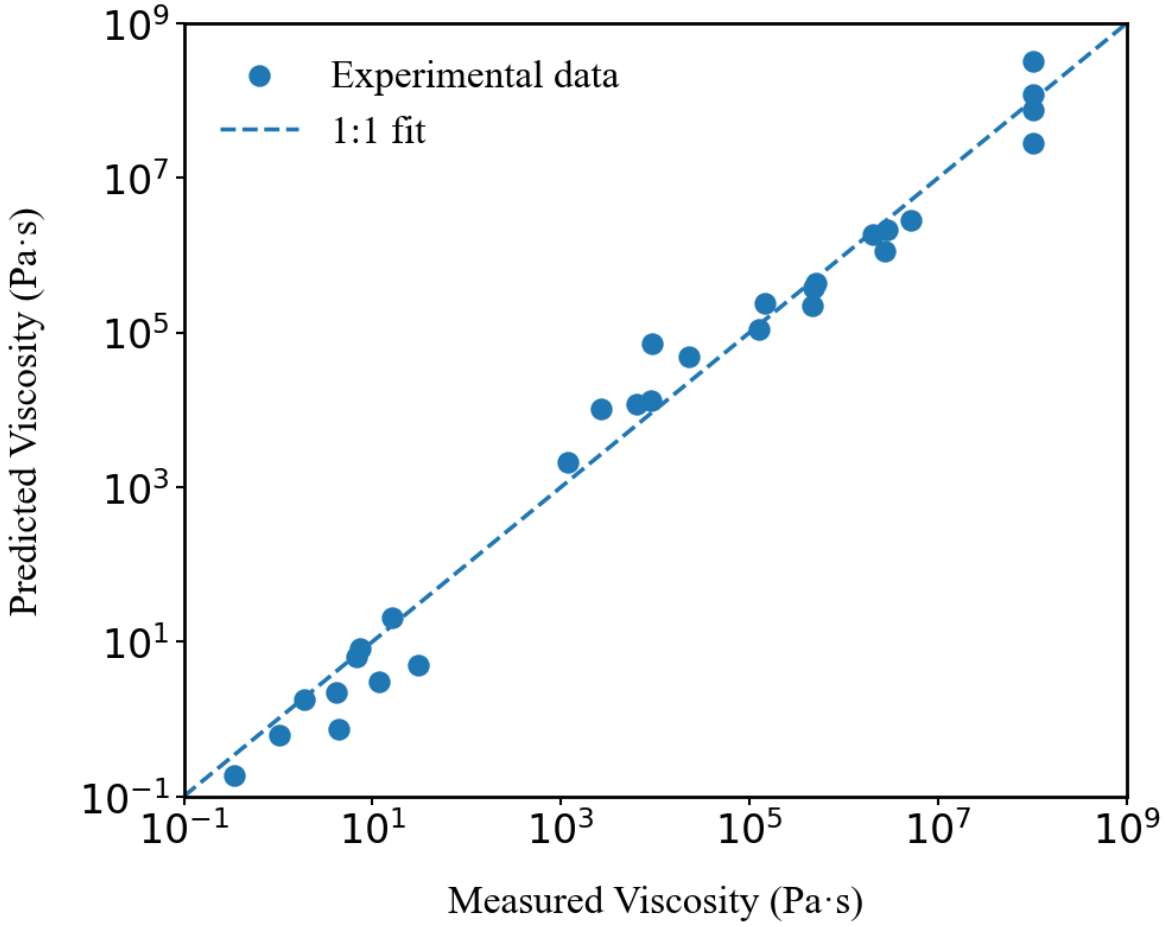

Figure S8. Comparison of experimental and predicted viscosity values for sucrose-H_2O droplets. The experimental values (blue circles) were measured between 273 and 303 K and ~20 to ~90% RH, whereas predicted viscosities (dashed line) were calculated using the VFT equation. The fitting procedure yields the fragility parameter (D_f) value of 13 ± 1.

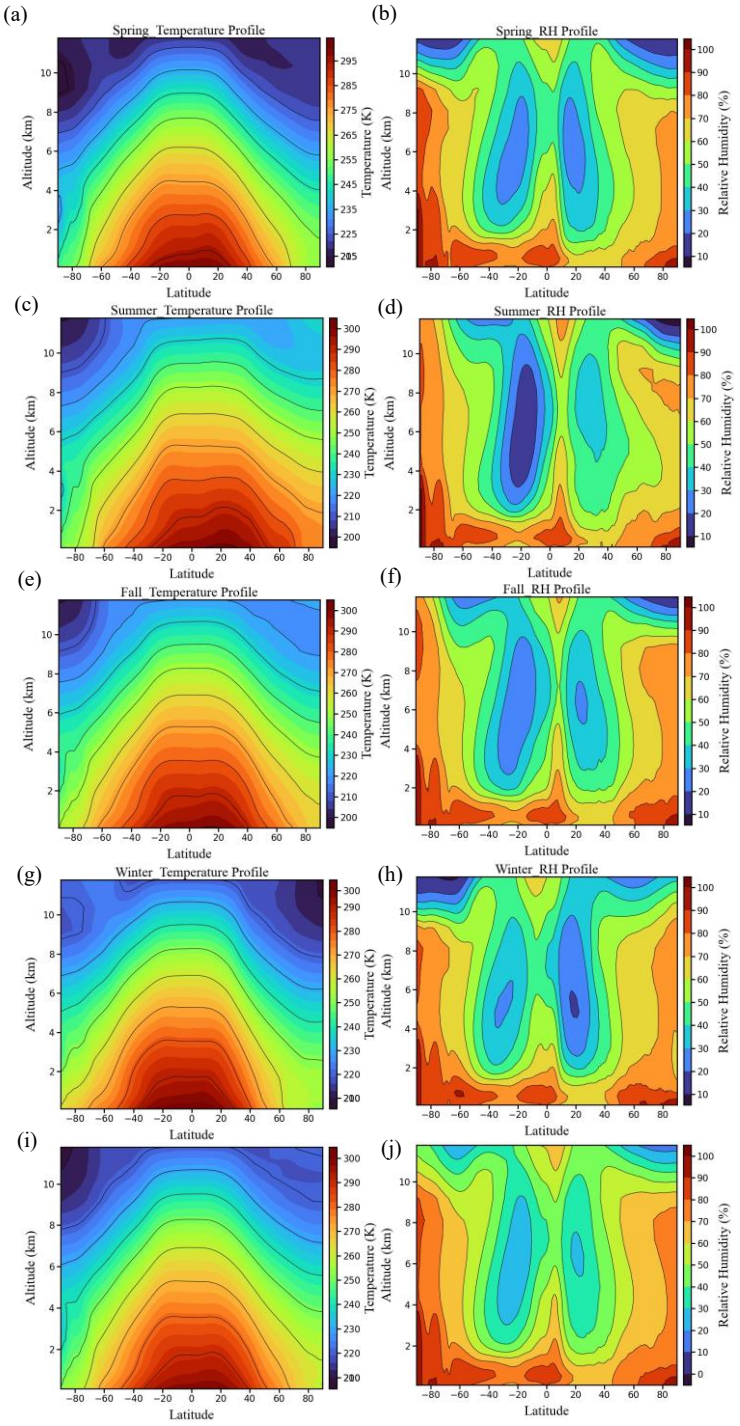
(a)
Spring_Temperature Profile
(b)
Spring_RH Profile
(c)
Summer_Temperature Profile
(d)
Summer_RH Profile
(e)
Fall_Temperature Profile
(f)
Fall_RH Profile
(g)
Winter_Temperature Profile
(h)
Winter_RH Profile
(i)
(j)
Altitude (km)
Latitude
Temperature (K)
Relative Humidity (%)

196

Figure S9. Altitude–latitude profiles of zonal-mean temperature and RH obtained from Copernicus Climate Data Store (https://cds.climate.copernicus.eu/), averaged seasonally and annually over the period 2020-01-01 to 2024-12-01. Panels present seasonal profiles for spring (a and b), summer (c and d), fall (e and f), and winter (g and h), showing temperature and RH, respectively. Panels (I and j) display the annual average zonal-mean profiles of temperature and RH.

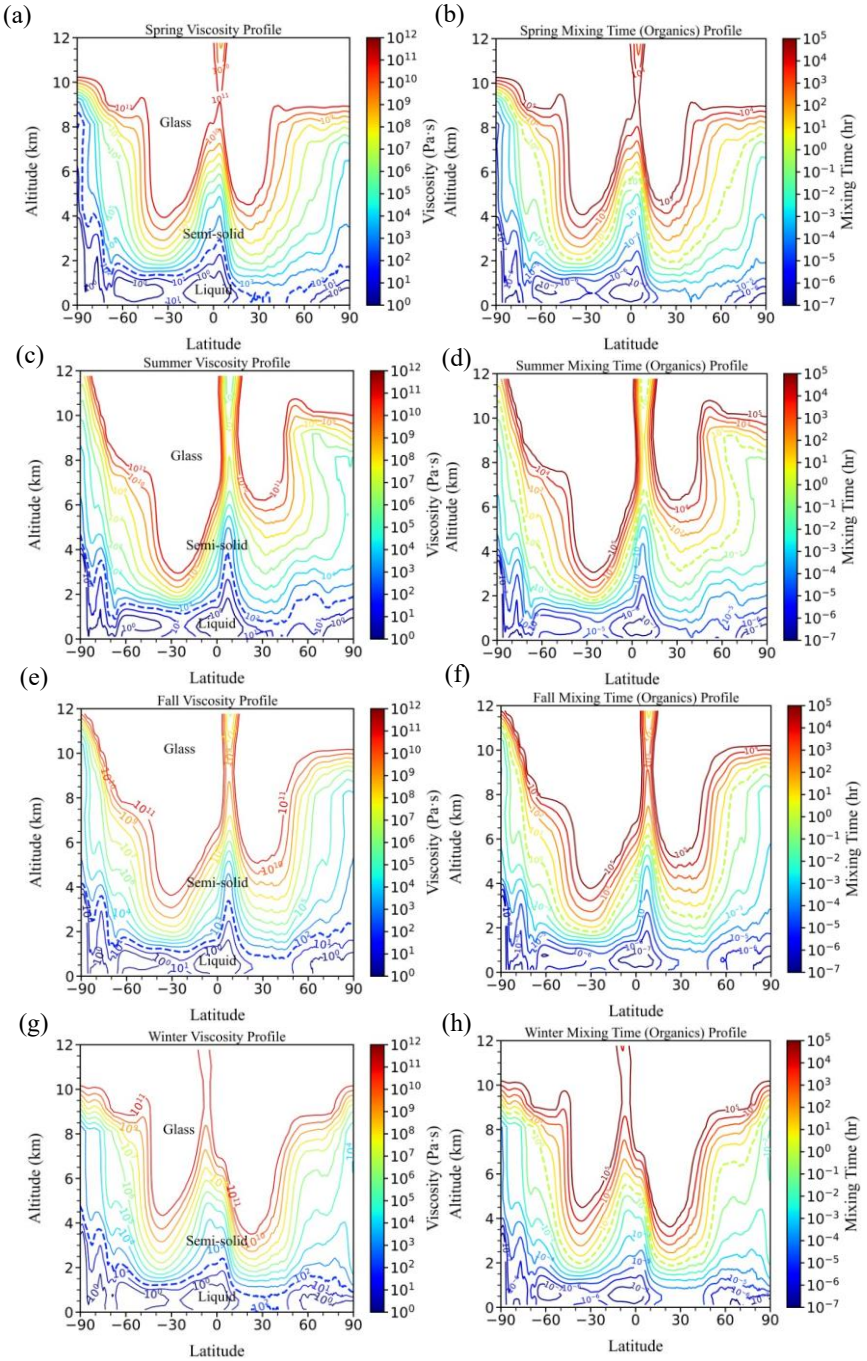
(a)
Spring Viscosity Profile
(b)
Spring Mixing Time (Organics) Profile
(c)
Summer Viscosity Profile
(d)
Summer Mixing Time (Organics) Profile
(e)
Fall Viscosity Profile
(f)
Fall Mixing Time (Organics) Profile
(g)
Winter Viscosity Profile
(h)
Winter Mixing Time (Organics) Profile
Glass
Semi-solid
Liquid
Altitude (km)
Latitude
Viscosity (Pa·s)
Mixing Time (hr)

201

Figure S10. Seasonal zonal-mean profiles of viscosity and mixing time of sucrose-H_2O droplets as a function of altitude and latitude, derived from temperature and RH data obtained from Copernicus Climate Data Store (https://cds.climate.copernicus.eu/) and averaged over the period 2020-01-01 to 2024-12-01. Panels (a and b) present viscosity and mixing time for spring, panels (c and d) for summer, panels (e and f) for fall, and panels (g and h) for winter. The blue dashed line shows the transition from liquid to semi-solid state. The light green dashed shows the mixing time of 1 hr.

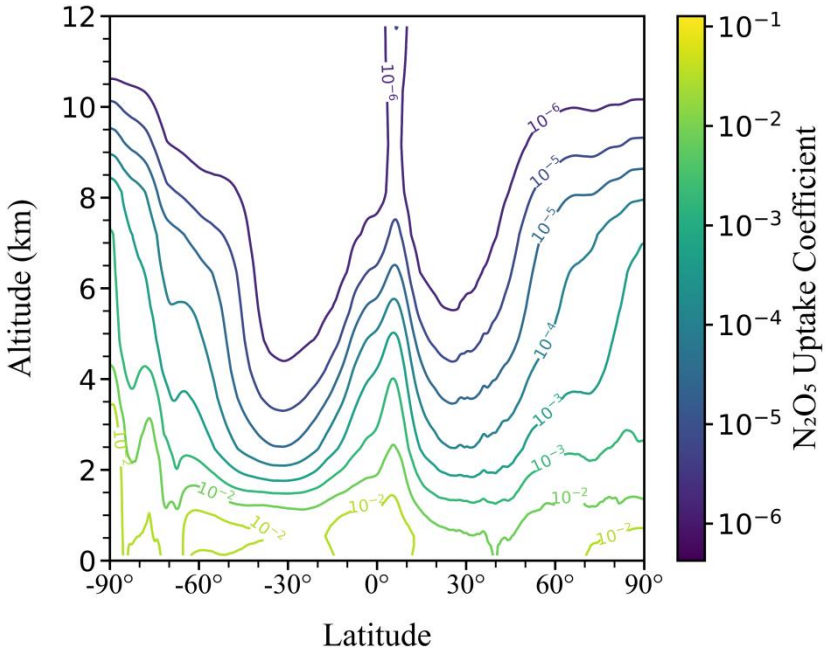

Figure S11. N_2O_5 uptake coefficient in 200 nm sucrose-H_2O droplets as a function of altitude and latitude based on annual average zonal-mean RH and temperature fields for the years 2020 to 2024, obtained from Copernicus Climate Data Store (https://cds.climate.copernicus.eu/). Surface hydrolysis is not considered in calculations of the N_2O_5 uptake coefficient (Γ_s is set to be 0 in Eq. S5.1).

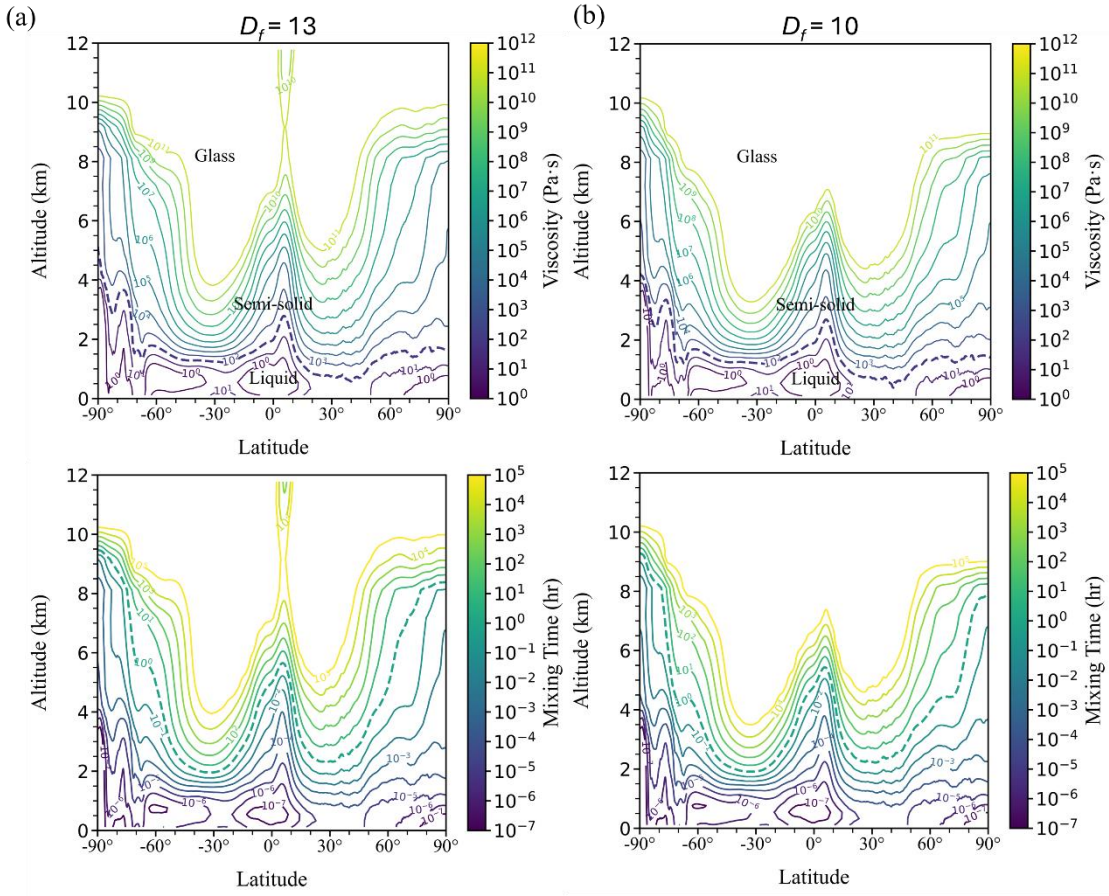

Figure S12. Influence of the fragility parameter D_f on the viscosity of sucrose-H_2O and related mixing-times in the troposphere. Panel (a) presents the viscosity of sucrose-H_2O and the mixing times calculated using D_f = 13, whereas panel (b) shows the corresponding profiles obtained with D_f = 10. All fields are shown as functions of altitude and latitude, derived from annual zonal-mean relative humidity and temperature for the years 2020–2024, obtained from the Copernicus Climate Data Store (https://cds.climate.copernicus.eu/).

Table S1. Summary of the conditioning time for sucrose-H_2O droplets measured at different temperatures and RH conditions. τ_{mix,H_2O} denotes the calculated characteristic mixing time of water, calculated from the diffusion coefficient of water from the viscosity inferred at the corresponding temperature and RH. $\tau_{conditioning}$ values represent the experimental conditioning time. Calculations were performed using the upper-limit droplet diameters employed in the experiments, namely 100 μm for bead-mobility experiments and 40 μm for poke-and-flow experiments.

RH	Particle dia. (μm)	$\tau_{conditioning}$ (h)	τ_{mix,H_2O} (h)	$\tau_{conditioning} / \tau_{mix,H_2O}$
Temp = 273 K				
79	100	3.30E-01	5.69E-03	58.0
53	40	1.50E+00	2.39E-01	6.3
49	40	1.50E+00	4.58E-01	3.3
Temp = 283 K				
81	100	1.60E-01	2.89E-03	55.3
76	100	1.60E-01	7.81E-03	20.5
55	40	1.00E+00	2.19E-02	45.7
49	40	1.00E+00	8.86E-02	11.3
46	40	1.00E+00	1.94E-01	5.1
42	40	1.00E+00	4.64E-01	2.2
Temp = 293 K				
90	100	1.60E-01	2.88E-04	555.7
86	100	1.60E-01	3.48E-04	459.8

83	100	1.60E-01	6.53E-04	245.1
79	100	1.60E-01	1.15E-03	139.0
75	100	1.60E-01	2.35E-03	68.1
71	100	1.60E-01	3.18E-03	50.4
50	40	5.00E-01	1.82E-02	27.5
44	40	5.00E-01	2.14E-02	23.3
39	40	5.00E-01	1.48E-01	3.4
34	40	5.00E-01	5.08E-01	1.0
Temp = 303 K				
73	100	1.60E-01	1.39E-03	115.5
69	100	1.60E-01	2.63E-03	60.7
65	100	1.60E-01	4.13E-03	38.7
50	40	5.00E-01	6.54E-03	76.5
44	40	5.00E-01	8.78E-03	56.9
39	40	5.00E-01	2.69E-02	18.6
34	40	5.00E-01	5.95E-02	8.4
29	40	5.00E-01	3.25E-01	1.5

231

232

233

References

Ammann, M., Cox, R. A., Crowley, J. N., Jenkin, M. E., Mellouki, A., Rossi, M. J., Troe, J., and Wallington, T. J.: Evaluated kinetic and photochemical data for atmospheric chemistry: Volume VI - heterogeneous reactions with liquid substrates, Atmos. Chem. Phys., 13, 8045–8228, https://doi.org/10.5194/acp-13-8045-2013, 2013.

Evoy, E.: The relationship between diffusion coefficients and viscosity in organic-water matrices as proxies for secondary organic aerosol, PHD thesis, The University of British Columbia, Vancouver, Canada, 2020.

Evoy, E., Kamal, S., Patey, G. N., Martin, S. T., and Bertram, A. K.: Unified description of diffusion coefficients from small to large molecules in organic–water mixtures, J. Phys. Chem. A, 124, 2301–2308, https://doi.org/10.1021/acs.jpca.9b11271, 2020.

Evoy, E., Kiland, K. J., Huang, Y., Schnitzler, E. G., Maclean, A. M., Kamal, S., Abbatt, J. P. D., and Bertram, A. K.: Diffusion coefficients and mixing times of organic molecules in β-caryophyllene secondary organic aerosol (SOA) and biomass burning organic aerosol (BBOA), ACS Earth Space Chem., 5, 3268–3278, https://doi.org/10.1021/acsearthspacechem.1c00317, 2021.

Evoy, E., Maclean, A. M., Rovelli, G., Li, Y., Tsimpidi, A. P., Karydis, V. A., Kamal, S., Lelieveld, J., Shiraiwa, M., Reid, J. P., and Bertram, A. K.: Predictions of diffusion rates of large organic molecules in secondary organic aerosols using the Stokes–Einstein and fractional Stokes–Einstein relations, Atmos. Chem. Phys., 19, 10073–10085, https://doi.org/10.5194/acp-19-10073-2019, 2019.

Galib, M. and Limmer, D. T.: Reactive uptake of N2O5 by atmospheric aerosol is dominated by interfacial processes, Science, 371, https://doi.org/10.1126/science.abd7716, 2021.

Grzinic, G., Bartels-Rausch, T., Berkemeier, T., Türler, A., and Ammann, M.: Viscosity controls humidity dependence of N2O5 uptake to citric acid aerosol, Atmos. Chem. Phys., 15, 13615–13625, https://doi.org/10.5194/acp-15-13615-2015, 2015.

Haynes, W. M.: CRC handbook of chemistry and physics, CRC press, https://doi.org/10.1201/9781315380476, 2016.

Hersbach, H., Bell, B., Berrisford, P., Biavati, G., Horányi, A., Muñoz Sabater, J., Nicolas, J., Peubey, C., Radu, R., and Rozum, I.: ERA5 monthly averaged data on pressure levels from 1940 to present, https://doi.org/10.24381/cds.6860a573, 2023.

Kiland, K. J., Mahrt, F., Peng, L., Nikkho, S., Zaks, J., Crescenzo, G. V., and Bertram, A. K.: Viscosity, glass formation, and mixing times within secondary organic aerosol from biomass burning phenolics, ACS Earth and Space Chem., 7, 1388–1400, https://doi.org/10.1021/acsearthspacechem.3c00039, 2023.

Maclean, A. M., Li, Y., Crescenzo, G. V., Smith, N. R., Karydis, V. A., Tsimpidi, A. P., Butenhoff, C. L., Faiola, C., Lelieveld, J., Nizkorodov, S. A., Shiraiwa, M., and Bertram, A. K.: Global distribution of the phase state and mixing times within secondary organic aerosol particles in the troposphere based on room-temperature viscosity measurements, ACS Earth Space Chem., 5, 3458–3473, https://doi.org/10.1021/acsearthspacechem.1c00296, 2021.

Petters, M. D. and Kreidenweis, S. M.: A single parameter representation of hygroscopic growth and cloud condensation nucleus activity, Atmos. Chem. Phys., 7, 1961–1971, https://doi.org/10.5194/acp-7-1961-2007, 2007.

Pöschl, U., Martin, S. T., Sinha, B., Chen, Q., Gunthe, S. S., Huffman, J. A., Borrmann, S., Farmer, D. K., Garland, R. M., Helas, G., Jimenez, J. L., King, S. M., Manzi, A. O., Mikhailov, E., Pauliquevis, T., Petters, M. D., Prenni, A. J., Roldin, P., Rose, D., Schneider, J., Su, H., Zorn, S. R., Artaxo, P., and Andreae, M. O.: Rainforest aerosols as biogenic nuclei of clouds and precipitation in the Amazon, Science, 329, 1513–1516, https://doi.org/10.1126/science.1191056, 2010.

Price, H. C., Mattsson, J., and Murray, B. J.: Sucrose diffusion in aqueous solution, Phys. Chem. Chem. Phys., 18, 19207–19216, https://doi.org/10.1039/c6cp03238a, 2016.

Riipinen, I., Pierce, J. R., Yli-Juuti, T., Nieminen, T., Hakkinen, S. A. K., Ehn, M., Junninen, H., Lehtipalo, K., Petäjä, T., Slowik, J. G., Chang, R. Y. W., Shantz, N., Abbatt, J. P. D., Leaitch, W. R., Kerminen, V. M., Worsnop,

D. R., Pandis, S. N., Donahue, N. M., and Kulmala, M.: Organic condensation: a vital link connecting aerosol formation to cloud condensation nuclei (CCN) concentrations, Atmos. Chem. Phys., 11, 3865–3878, https://doi.org/10.5194/acp-11-3865-2011, 2011.

Sellier, M., Grayson, J. W., Renbaum-Wolff, L., Song, M., and Bertram, A. K.: Estimating the viscosity of a highly viscous liquid droplet through the relaxation time of a dry spot, J. Rheol., 59, 733–750, https://doi.org/10.1122/1.4917240, 2015.

Smith, N. R., Crescenzo, G. V., Huang, Y., Hettiyadura, A. P. S., Siemens, K., Li, Y., Faiola, C., Laskin, A., Shiraiwa, M., Bertram, A. K., and Nizkorodov, S. A.: Viscosity and liquid–liquid phase separation in healthy and stressed plant SOA, Environ. Sci. Atmos., 1, 140–153, https://doi.org/10.1039/d0ea00020e, 2021.

Weight, W. D.: Practical Hydrogeology: Principles and field applications, McGraw Hill Professional, Newyork, 2019.

Winston, P. W. and Bates, D. H.: Saturated solutions for the control of humidity in biological research, Ecology, 41, 232–237, https://doi.org/10.2307/1931961, 1960.